Title
Putative Microcircuit-Level Substrates for Attention Are Disrupted in Mouse Models of Autism

Journal
Biological Psychiatry, 79(8)

ISSN
0006-3223

Authors
Luongo, Francisco J
Horn, Meryl E
Sohal, Vikaas S

Publication Date
2016-04-01

DOI
10.1016/j.biopsych.2015.04.014

Peer reviewed

HHS Public Access

Author manuscript

Biol Psychiatry. Author manuscript; available in PMC 2017 April 15.

Published in final edited form as:

Biol Psychiatry. 2016 April 15; 79(8): 667–675. doi:10.1016/j.biopsych.2015.04.014.

Putative microcircuit-level substrates for attention are disrupted in mouse models of autism

Francisco Luongo[1,2,3,4], **Meryl Horn**[4], and **Vikaas S. Sohal**[1,2,3,*]

[1]Department of Psychiatry, 675 Nelson Rising Lane University of California, San Francisco San Francisco, CA 94143-0444

[2]Center for Integrative Neuroscience, 675 Nelson Rising Lane University of California, San Francisco San Francisco, CA 94143-0444

[3]Sloan-Swartz Center for Theoretical Neurobiology, 675 Nelson Rising Lane University of California, San Francisco San Francisco, CA 94143-0444

[4]Neuroscience Graduate Program, 675 Nelson Rising Lane University of California, San Francisco San Francisco, CA 94143-0444

Abstract

BACKGROUND—Deep layer excitatory circuits in the prefrontal cortex represent the strongest locus for genetic convergence in autism, but specific abnormalities within these circuits that mediate key features of autism, such cognitive or attentional deficits, remain unknown. Attention normally increases the sensitivity of neural populations to incoming signals by decorrelating ongoing cortical circuit activity. Here we investigated whether mechanisms underlying this phenomenon might be disrupted within deep layer prefrontal circuits in mouse models of autism.

METHODS—We isolated deep layer prefrontal circuits in brain slices then used single-photon GCaMP imaging to record activity from many (50-100) neurons simultaneously, in order to study patterns of spontaneous activity generated by these circuits under normal conditions and in two etiologically distinct models of autism: mice exposed to valproic acid (VPA) *in utero* and *FMR1* KO mice.

RESULTS—We found that modest doses of the cholinergic agonist carbachol normally decorrelate spontaneous activity generated by deep layer prefrontal networks. This effect was disrupted in both VPA-exposed and *FMR1* KO mice, but intact following other manipulations which do not model autism.

CONCLUSIONS—Our results suggest that cholinergic modulation may contribute to attention by acting on local cortical microcircuits to decorrelate spontaneous activity. Furthermore, defects

* To whom correspondence should be addressed at vikaas.sohal@ucsf.edu.

FINANCIAL DISCLOSURES

All authors report no biomedical financial interests or potential conflicts of interest.

in this mechanism represent a microcircuit-level endophenotype that could link diverse genetic and developmental disruptions to attentional deficits in autism. Future studies could elucidate pathways leading from various etiologies to this circuit-level abnormality, or use this abnormality itself as a target, and identify novel therapeutic strategies that restore normal circuit function.

Keywords

calcium imaging; GCaMP; prefrontal cortex; Fragile X syndrome; acetylcholine; valproic acid

INTRODUCTION

Autism reflects disparate genetic and environmental causes, suggesting that common behavioral phenotypes may reflect convergent defects at the level of neuronal circuits controlling these behaviors. Consistent with this hypothesis, recent analyses have revealed that several genes linked to autism are co-expressed within deep layer microcircuits in the prefrontal cortex (PFC) (1, 2). Identifying convergent abnormalities located within these microcircuits would yield attractive targets for future circuit-based therapeutic interventions. Until recently, a major barrier to identifying such circuit-level abnormalities has been recording from large numbers of neurons simultaneously. However, advances in imaging and electrophysiological techniques have made it possible to characterize patterns of circuit-level activity by, for example, calculating correlations between neurons (3, 4). Despite these advances, cognitive processes are associated with complex neural dynamics embedded within a high dimensional state space. Thus, in order to reveal defects in circuit-level activity that are associated with disorders such as autism, it is valuable to first identify specific neuronal correlates or signatures for relevant cognitive processes. Identifying these signatures makes it possible to evaluate whether they are altered in the setting of diseases such as autism. Any such alterations represent putative pathophysiological mechanisms contributing to cognitive dysfunction in these disease states.

Here, we set out to identify possible microcircuit-level abnormalities associated with autism. Our approach was to look for convergent abnormalities that are 1) conserved across multiple, etiologically distinct models of autism, and 2) impact neural correlates of cognitive processes that are known to be abnormal in autism. In particular, two recent studies identified a possible neural signature of attention using multi-neuronal recording in monkeys performing a visuospatial attention task (5, 6). Both studies observed the same result: during the attended portion of the task, the pairwise correlations between cortical neurons *decreased*. This decorrelation would reduce the overall noise of an output signal that was composed of a sum across the population – in fact, this pairwise decorrelation accounted for 80% of the total improvement in the signal-to-noise ratio (6). This phenomenon is hypothesized to reflect the decorrelation of spontaneous network activity by neuromodulation. In particular, cholinergic modulation plays a well-established role in attention and cortical decorrelation *in vivo* (7). Nevertheless, it remains unknown whether cholinergic modulation can induce such decorrelations by acting directly on cortical microcircuits and if so, whether defects in this mechanism might be present in autism or other conditions with a high comorbidity of attentional deficits. Notably, in Fragile X syndrome (the most common known single gene cause of autism), 70% of affected children

meet criteria for an attentional deficit (8). Overall, approximately 50% of children with autism also meet criteria for attention deficit hyperactivity disorder (8). Deficits in attention have also been observed in *FMR1* KO mice (9-11) and other mouse models of autism (12).

To examine how autism might affect a neural correlate of attention, we studied how cholinergic modulation affects spontaneous activity generated by deep layer prefrontal microcircuits under normal conditions and in mouse models of autism. We focused on microcircuits in deep layers of the PFC because cholinergic modulation within the PFC has been directly implicated in attention (13, 14), and abnormalities associated with autism are likely to be intrinsic to deep layer prefrontal microcircuits (1). Therefore, we isolated these microcircuits in brain slices, and used single-photon, wide field GCaMP imaging (15) to measure spontaneous activity in many neurons (50-100) at once. As described below, we found that cholinergic modulation can indeed act directly on cortical microcircuits to decorrelate spontaneous activity, mimicking the neural signature previously linked to attention *in vivo*. Furthermore, this decorrelation, which represents a possible neural substrate for attention, is defective in two etiologically distinct mouse models of autism.

MATERIALS AND METHODS

All experiments were conducted in accordance with procedures established by the Administrative Panels on Laboratory Animal Care at the University of California, San Francisco.

Subjects

P26-33 mice of either sex (Charles River) were injected unilaterally with 500 nL of AAV5/2—synapsin::GCaMP6s (UNC viral vector core) at the coordinates (in mm): 1.7 anterior-posterior (AP), 0.3 mediolateral (ML), and −2.2 dorsoventral (DV). Experiments studying the valproic acid (VPA) model of autism used C57BL/6 mice whose pregnant mothers had been injected with a single dose of VPA (500 mg/kg i.p.) at E10.5. For these experiments, control mice were C57BL/6 mice whose pregnant mothers had been injected with saline at E10.5. VPA solution was prepared by dissolving VPA in 0.9% saline to a final concentration of 150 mg/mL. Experiments studying a mouse model of Fragile X syndrome used male *FMR1* WT or KO mice on a FVB background (Jackson labs). In some cases (active ACSF cohorts), these *FMR1* WT and KO mice were littermates, while others (carbachol cohorts) were not.

For some experiments, C57Bl/6 mice were treated with fluoxetine based on a previously described protocol (16). Fluoxetine was administered (5 mg kg^{-1}, I.P.) once daily for 6 days prior to imaging with the final injection coming 24-48 hours before imaging. Dominant negative DISC1 mutant mice were generated by crossing B6-CamKII::TtA (JAX: 00310) mice with tetO-DISC1dn (JAX: 008790) to yield mice expressing dominant negative DISC1 in neocortical pyramidal cells.

Slice preparation

In all cases, 350 micron thick coronal slices were prepared from these animals 15-27 days after injection (6-8 weeks of age). Slices preparation followed our previously described

protocol (17) with one deviation: immediately after brain slices were prepared, they were transferred to an N-Methyl-D-Glucamine (NMDG)-based recovery solution for 10 min before being transferred to ACSF for the remainder of their recovery (18). The NMDG-based solution was maintained at 32° C, and consisted of the following (in mM): 93 N-Methyl-D-Glucamine (NMDG), 93 HCl, 2.5 KCl, 1.2 NaH2PO4, 30 NaHCO3, 25 glucose, 20 HEPES, 5 Na-ascorbate, 5 Na-pyruvate, 2 thiourea, 10 magnesium sulfate, 0.5 calcium chloride. This NMDG preparation method was used to improve the overall health of adult slices to ensure sufficient amounts of activity for analysis. ACSF contained the following (in mM): 126 NaCl, 26 NaHCO3, 2.5 KCl, 1.25 NaH2PO4, 1 MgCl2, 2 CaCl, and 10 glucose. All recordings were at 32.5 +/− 1°C. “Active” ACSF was identical to normal ACSF except with elevated KCl (3.5mM vs. 2mM) and reduced CaCl (1.2mM vs. 2mM).

Imaging

GCaMP imaging was performed on an Olympus BX51 upright microscope with a 20× 1.0NA water immersion lens, 0.5× reducer (Olympus), and ORCA-ER CCD Camera (Hamamatsu Photonics). Illumination was delivered using a Lambda DG4 arc lamp (Sutter Instruments). Light was delivered through a 472/30 excitation filter, 495nm single band dichroic, and 496nm long pass emission filter (Semrock).

All movies that were analyzed consisted of 36000 frames acquired at 10Hz (1 hr) with 4×4 sensor binning yielding a final resolution of 256 × 312 pixels. Light power during imaging was 100 – 500 μW/mm^2. The Micro Manager software suite (v1.4, NIH) was used to control all camera parameters and acquire movies Any movies that had significant drift (greater than ~0.25 soma diameters), movement, or lacked significant amounts of activity were excluded from further analysis. Significant movement could be detected during independent components analysis (ICA) by the appearance of elliptical rather than circular segments. We observed that active, GCaMP-expressing neurons were found within a discrete layer (c.f. Fig. 1A) consistent with the location of layer 5 in medial prefrontal cortex.

Signal extraction

All analyses and signal extraction was performed using MATLAB (Mathworks). Locations of cells were automatically identified using a modified version of the published CellSort 1.1 toolbox (19). In particular, a factor, μ, specifies the weight between spatial and temporal sparseness: $\mu = 0$ is purely spatial and $\mu = 1$ is purely temporal. All of our analyses used $\mu = 0.2$ which was within the optimal range outlined in (19). Signals were extracted from movies and the baseline fluorescence function, F_0, was calculated for every trace using the mode of the kernel density estimate over a 100s rolling window, implemented via the MATLAB function ksdensity following the procedure outlined in (20). All signal traces shown represent normalized versions of the $(F\text{-}F_0)/F_0$ trace.

Threshold based event detection was performed on the traces by detecting increases in $(F\text{-}F_0)/F_0$ exceeding 2.5σ over one second, and then further thresholding these events by keeping only those events which exceeded a 4σ increase over two seconds. σ is the standard deviation of $(F\text{-}F_0)/F_0$, calculated over the entire movie. Thus all detected events have a deviation of at least 4σ from baseline. After identifying these events in the calcium signal

from a cell, the cell was considered "active" during the entire period from the beginning to the peak of the event. The beginning of the event was defined as the first point for which $(F-F_0)/F_0$ increases by 2.5σ within 1 second and by 4σ within 2 seconds. The peak of the event was defined as the local maximum of the entire event, from the beginning of the event until $(F-F_0)/F_0$ returns to the same baseline value. We then created a matrix in which each row corresponds to a neuron, and each column corresponds to a frame. Entries in this matrix were 1 if a given neuron was active during a given frame, and 0 otherwise. All subsequent analyses were performed on this two-dimensional representation of network activity over time (c.f. Fig. 1C).

Correlations between cells were calculated between the binary event trains corresponding to those two cells after subtracting the mean level of activity from each event train.

The standard deviation projection in Figure 1 was obtained as follows. For each pixel, we computed the standard deviation of $(F-F_0)/F_0$ over 30 second intervals throughout the first 10 minutes of a movie, then plotted the maximum value of these standard deviations.

Statistical analysis

Unless otherwise noted, we used the Mann Whitney U-test to compare pairs of groups, repeated measures ANOVA to compare multiple groups, and the two-tailed Kolmogorov-Smirnov (KS) test to compare pairs of distributions. To compare the number of strong correlations between conditions, we treated the fraction of strong correlations in each slice as an observation. Error bars where shown indicate standard error unless otherwise noted. Cell identification, signal extraction and normalization, event detection, and all other data analysis was done using fully automated routines that were independent of the investigator and thus blinded.

RESULTS

We recorded sparse, robust GCaMP signals from neurons in layer 5 (L5) of the medial prefrontal cortex (mPFC; Fig. 1) in acute brain slices from late adolescent (P41-57) mice (n = 95). Using a combination of independent component analysis (ICA) and image segmentation (19), we located neurons, measured their GCaMP signals, and detected events corresponding to increased activity in these neurons (Fig. 1A-C). Each experiment recorded from 50-100 active L5 neurons for 1 hour. Table 1 lists all of our experiments, performed in control mice or mice modeling autism or other manipulations, and using either carbachol or high K^+ ACSF to elicit spontaneous activity. Table 1 also includes summary statistics for each set of experiments.

We first sought to demonstrate the presence of correlated activity within our datasets. Experiments contained more strong correlations than shuffled datasets, in which the event train for each neuron is shifted in time by a different random amount, or scrambled datasets, in which the neuronal identities associated with each event are randomly reassigned (Fig 1D). Shuffled datasets preserve the temporal structure of activity within each neuron, whereas scrambled datasets preserve the number of neurons active at any given point in time, thus maintaining the temporal structure of activity at the network level. We set an

arbitrary threshold of 0.15, and quantified the fraction of correlations exceeding this threshold. As shown in Fig. 1D, correlations exceeding this threshold were present at negligible levels in shuffled or scrambled datasets, so we used this threshold to define "strong" correlations, i.e. correlations which exceed those expected simply by chance.

Given the posited link between cholinergic modulation and cortical circuit decorrelation, we next compared spontaneous prefrontal microcircuit activity elicited by 2 μM carbachol to activity in "active ACSF" (21), which contains relatively high K^+ and low Ca^{2+}. Active (or high K^+) ACSF elicits similar levels of spontaneous activity as 2 μM cabrachol (avg % time active = 4.2 ± 0.3 in carbachol vs. 4.5 ± 0.5 in high K^+), making it possible to compare the properties of such activity when cholinergic modulation is present or absent, independent of changes in activity levels. These experiments, comparing recordings in carbachol to those in high K^+, were all done using WT mice on an FVB background, which served as controls for experiments with *FMR1* KO mice described below. Consistent with our hypothesis that cholinergic modulation decorrelates prefrontal microcircuit activity, the distribution of pairwise correlations was shifted to the right in high K^+ compared to carbachol (Fig. 2A). This resulted in a marked increase in the fraction of "strong" correlations (correlations >0.15), from 1.2 ± 0.3% in carbachol to 4.0 ± 0.9% in high K^+ (Fig. 2A inset).

Notably the decrease in correlations observed in carbachol was not an artifact of differences in activity. Plotting the fraction of strong correlations against the mean % time activity for each experiment in carbachol or high K^+ shows that the fraction of strong correlations is increased in high K^+ compared to carbachol, for all activity levels (Fig. 2D). To quantitatively and explicitly account for possible confounding effects of activity on the prevalence of strong correlations, we performed linear regression (Fig. 2D), and computed the difference between the observed fraction of strong correlations and the number expected based simply on the level of activity. These residual values are shown in Fig. 2E, and confirm that even when activity levels are taken into account, correlations in high K^+ are stronger than those in carbachol.

Next, we examined whether this carbachol-induced decorrelation, which represents a possible biological substrate for attention, might be disrupted in in two etiologically dissimilar mouse models of autism. First, we studied mice exposed to valproic acid (VPA) *in utero* at E10.5 (Methods). VPA is an anticonvulsant and mood stabilizer, and there is a markedly elevated rate of autism in the children of mothers treated with VPA (but not other anticonvulsants) during pregnancy (22-24). Rodents exposed to VPA *in utero* exhibit numerous autism-like phenotypes (25, 26). We also studied *FMR1* KO mice, which model Fragile X syndrome, the most common known genetic cause of autism (27).

In stark contrast to the carbachol-induced decorrelation described earlier, in both VPA-exposed and *FMR1* KO slices, carbachol failed to elicit a leftward shift of the correlation distribution (Fig. 2B,C). In fact, carbachol *increased* correlations in the VPA-exposed microcircuits (Fig. 2C). A potentially complicating factor is that unlike the case in wild-type slices, in both VPA-exposed and *FMR1* KO slices, levels of activity were lower in carbachol compared to high K^+ ACSF. We calculated correlations using mean subtracted even trains, which should minimize activity level-dependent effects. Indeed, as Fig. 2D shows, there is at

best a very weak relationship between activity levels and correlations. We also carried out additional analyses described in the Supplemental Information which confirm that the absence of a carbachol-induced decorrelation in autism models was not simply an artifact of differences in activity levels (Fig. S1).

We reasoned that this loss of the carbachol-induced decorrelation should cause correlations during carbachol-induced activity to be higher in models of autism compared to controls. We compared VPA-exposed mice to age-matched controls whose mothers had been injected with saline at the same timepoint. For *FMR1* KO mice, we used age-matched *FMR1* WT controls. In carbachol, both autism models exhibit a significant increase in the fraction of strong correlations relative to controls (Fig. 3A,B). Notably, levels of carbachol-induced activity were essentially identical in *FMR1* WT and KO mice (4.2 ± 0.3% and 4.3 ± 0.4% in WT and KO respectively), demonstrating that the abnormally high correlations we observed during carbachol-induced activity in *FMR1* KO mice are not simply an artifact of differences in activity. By contrast, levels of carbachol-induced activity were different for VPA-exposed mice and their wildtype controls, but once again, accounting for these differences could not explain the abnormally increased strong correlations observed in VPA-exposed mice (Fig. S2C; Fig. S3).

Finally, we evaluated whether this abnormal increase in correlations during carbachol-induced activity possesses specificity for autism. For this, we examined genetic and pharmacologic perturbations that affect the PFC but do not model autism: mice expressing a dominant negative version of DISC1 in excitatory neurons (CaMKII-TTA / TetO-dnDISC1), and mice chronically treated with the commonly prescribed selective-serotonin reuptake inhibitor fluoxetine. DISC1 disruption models aspects of schizophrenia and depression, including behaviors related to PFC dysfunction, e.g. impaired working memory and decreased social interaction (28-30). Chronic treatment with fluoxetine alters cell proliferation in the mPFC (31) in ways that may contribute to its effects on depression-like and repetitive behaviors. If the changes we saw in VPA-exposed and *FMR1* KO mice were simply nonspecific consequences of perturbing PFC microcircuits, then we would expect these other mice to exhibit a similar increase in correlations during carbachol-induced activity. However, we observed no such increase in correlations during carbachol-induced activity in either of these cases compared to controls (Fig. 3C, D).

DISCUSSION

In this study we have identified a putative microcircuit level-phenotype associated with autism: a defect in the ability of cholinergic modulation to decorrelate spontaneous cortical circuit activity. We show that this decorrelation, previously observed *in vivo*, can also be observed at the level of isolated cortical microcircuits, and that it is lost in two mouse models of autism. Lastly, we show that this defect is at least somewhat specific for autism, as it is not present following two other manipulations that affect prefrontal cortex: chronic treatment with fluoxetine, and expression of a dominant-negative form of DISC1. This suggests that the loss of cholinergic-dependent decorrelation observed might represent a microcircuit-level phenotype with specificity for autism, and thus could constitute an attractive target for novel circuit level-therapies.

Relationship to in vivo studies

While we have shown the cholinergic decorrelation to be present *in vitro*, it will be important to compare our findings to features of activity occurring *in vivo*. That being said, *in vivo* recordings address fundamentally different questions from those addressed here. Activity *in vivo* is strongly influenced by synaptic inputs originating outside the local microcircuit as well as factors such as behavior state. Thus, while *in vivo* studies are uniquely able to identify network phenomena, e.g., decorrelations recruited by attention (5, 6) and acetylcholine (7), they are not well suited for determining how these phenomena relate to local microcircuit mechanisms. For example, even if it were possible to precisely control levels of neuromodulation *in vivo*, doing so would almost certainly elicit confounding changes in feedforward and feedback inputs. Here, by studying isolated microcircuits within brain slices, we demonstrate unequivocally that the decorrelations observed *in vivo* can emerge as a result of cholinergic modulation acting directly on microcircuits. (Interestingly, whereas we studied ongoing patterns of spontaneous network activity similar to those believed to mediate attentional effects *in vivo*, another recent *in vitro* study (4) showed that acetylcholine decorrelates the latency to the first spike in somatosensory neurons responding to thalamic input).

We go on to demonstrate that the carbachol-induced decorrelation of spontaneous network activity we found is disrupted in models of autism. If one observed abnormal correlations in models of autism *in vivo*, it would be unclear whether these abnormalities reflect the inability of cholinergic modulation to decorrelate local circuits (as we have found) vs. more macroscopic deficits, e.g. the inability of these animals to engage the appropriate behavioral state. Our approach is specifically intended to isolate and examine the integrity of specific microcircuit mechanisms, in a way that complements *in vivo* work. Our focus on mechanisms that are intrinsic to deep layer prefrontal circuits is particularly relevant given that these circuits represent the single strongest locus of convergence for autism genes (1).

Relevance to autism

Great progress has been made in identifying genes and environmental factors that contribute to autism. However, it has been challenging to understand how all of these “add up” to alter circuit activity in ways that could impact behavior. Cortical microcircuits, within which many cell types and synapses interact to generate patterns of neural activity, represent an attractive locus at which at which many different genetic, environmental, and developmental lesions could converge to elicit common phenotypes. Thus, many studies have begun exploring possible circuit-level endophenotypes for complex neuropsychiatric disorders including autism (32-34).

As discussed above, attentional deficits are a major feature of autism generally, and Fragile X syndrome in particular. The failure of cholinergic modulation to decorrelate PFC microcircuit activity in autism models holds face validity as a possible contributor to these deficits. The presence of this same abnormality in two models of autism with very different etiologies (but not in association with other manipulations of prefrontal function) provides additional empirical validity for the hypothesis that this abnormality plays a role in the pathophysiology of autism. Importantly, this circuit-level abnormality may come about as a

result of multiple, dissimilar cellular and synaptic effects in *FMR1* KO and VPA-exposed mice. Indeed, as stated earlier, numerous autism-related genes are convergently expressed within the deep layer PFC circuits we have shown are abnormal (1). This highlights the importance of identifying microcircuit-level phenotypes, such as the loss of cholinergic decorrelation, that could represent convergent consequences of disruptions in multiple genes, and which could plausibly contribute to common aspects of autism, e.g. attentional deficits.

Possible circuit mechanisms

Of course, it will still be important to identify the cellular and/or synaptic actions of cholinergic modulation which normally help desynchronize microcircuit activity, but are abnormal in VPA-exposed and/or *FMR1* KO mice. Various studies have shown that cholinergic modulation can increase the excitability of interneurons which express somatostatin or vasoactive intestinal peptide (35, 36), hyperpolarize fast-spiking interneurons (36), regulate short-term plasticity at both excitatory and inhibitory synapses (37), preferentially elicit persistent firing in subcortically-projecting (vs. callosally-projecting) L5 pyramidal neurons (38), and suppress intracortical (but not thalamocortical) excitatory synapses (39). Of course, it remains unclear whether each of these effects is present in the prefrontal circuits we have studied, contributes to the cholinergic-ineduced decorrelation we have found, and/or is altered in *FMR1* KO and VPA-exposed mice.

Rather than to explore each of these effects individually, we instead took the unconventional approach of developing a new assay, using it to examine whether all the effects of cholinergic modulation add up to exert some net influence on circuit activity, and then evaluating whether that net circuit-level influence is altered in a consistent way across VPA-exposed and *FMR1* KO mice. Examining individual cellular and synaptic effects of cholinergic modulation would be time consuming, and might miss the “big picture” of how diverse abnormalities can add up to elicit a common, circuit-level phenotype. By contrast, the approach demonstrated here can explore how various factors shape pairwise decorrelation and other emergent network properties. For example, one could combine optogenetic inhibition of genetically targeted cell populations with GCaMP imaging to explore how specific cell types influence network correlation / decorrelation.

Conclusions

By describing a potential new microcircuit-level phenotype for autism, our study builds a critical foundation for future work to elucidate the detailed pathways, leading from the *FMR1* gene or VPA exposure, to the abnormal response of prefrontal microcircuits to cholinergic modulation we have found. One could also evaluate potential therapies by measuring how well they improve the ability of cholinergic modulation to decorrelate these circuits – this approach might reveal novel therapeutic strategies that bypass the molecular pathways disrupted in autism, and instead exploit alternative mechanisms to normalize overall circuit function.

Supplementary Material

Refer to Web version on PubMed Central for supplementary material.

ACKNOWLEDGEMENTS

This work was supported by the Staglin Family and International Mental Health Research Organization (IMHRO), Simons Foundation for Autism Research, Alfred P. Sloan Foundation, NIMH (R00MH085946), and NIH Office of the Director (DP2MH10001101). FL received support from an IMSD fellowship from NIGMS (R25GM56847). Tosha Patel and Audrey Brumback provided VPA-exposed mice. Philip Sabes and Michael Stryker provided helpful comments on the manuscript. We also acknowledge the use of GCaMP constructs developed by Vivek Jayaraman, Rex Kerr, Douglas Kim, Loren Looger, and Karel Svoboda as part of the GENIE Project at the Janelia Farm Research Campus, Howard Hughes Medical Institute.

REFERENCES

1. Willsey AJ, Sanders SJ, Li M, Dong S, Tebbenkamp AT, Muhle RA, et al. Coexpression networks implicate human midfetal deep cortical projection neurons in the pathogenesis of autism. Cell. 2013; 155:997–1007. [PubMed: 24267886]
2. Chang J, Gilman SR, Chiang AH, Sanders SJ, Vitkup D. Genotype to phenotype relationships in autism spectrum disorders. Nat Neurosci. 2014
3. Sadovsky AJ, MacLean JN. Scaling of topologically similar functional modules defines mouse primary auditory and somatosensory microcircuitry. J Neurosci. 2013; 33:14048–14060. 14060a. [PubMed: 23986241]
4. Runfeldt MJ, Sadovsky AJ, MacLean JN. Acetylcholine Functionally Reorganizes Neocortical Microcircuits. J Neurophysiol. 2014
5. Mitchell JF, Sundberg KA, Reynolds JH. Spatial attention decorrelates intrinsic activity fluctuations in macaque area V4. Neuron. 2009; 63:879–888. [PubMed: 19778515]
6. Cohen MR, Maunsell JH. Attention improves performance primarily by reducing interneuronal correlations. Nat Neurosci. 2009; 12:1594–1600. [PubMed: 19915566]
7. Goard M, Dan Y. Basal forebrain activation enhances cortical coding of natural scenes. Nat Neurosci. 2009; 12:1444–1449. [PubMed: 19801988]
8. (!!! INVALID CITATION !!!)
9. Moon J, Beaudin AE, Verosky S, Driscoll LL, Weiskopf M, Levitsky DA, et al. Attentional dysfunction, impulsivity, and resistance to change in a mouse model of fragile X syndrome. Behav Neurosci. 2006; 120:1367–1379. [PubMed: 17201482]
10. Casten KS, Gray AC, Burwell RD. Discrimination learning and attentional set formation in a mouse model of Fragile X. Behav Neurosci. 2011; 125:473–479. [PubMed: 21517146]
11. Dickson PE, Corkill B, McKimm E, Miller MM, Calton MA, Goldowitz D, et al. Effects of stimulus salience on touchscreen serial reversal learning in a mouse model of fragile X syndrome. Behav Brain Res. 2013; 252:126–135. [PubMed: 23747611]
12. McTighe SM, Neal SJ, Lin Q, Hughes ZA, Smith DG. The BTBR mouse model of autism spectrum disorders has learning and attentional impairments and alterations in acetylcholine and kynurenic acid in prefrontal cortex. PLoS One. 2013; 8:e62189. [PubMed: 23638000]
13. Dalley JW, Cardinal RN, Robbins TW. Prefrontal executive and cognitive functions in rodents: neural and neurochemical substrates. Neurosci Biobehav Rev. 2004; 28:771–784. [PubMed: 15555683]
14. Parikh V, Sarter M. Cholinergic mediation of attention: contributions of phasic and tonic increases in prefrontal cholinergic activity. Ann N Y Acad Sci. 2008; 1129:225–235. [PubMed: 18591483]
15. Tian L, Hires SA, Mao T, Huber D, Chiappe ME, Chalasani SH, et al. Imaging neural activity in worms, flies and mice with improved GCaMP calcium indicators. Nature methods. 2009; 6:875–881. [PubMed: 19898485]

16. Welch JM, Lu J, Rodriguiz RM, Trotta NC, Peca J, Ding JD, et al. Cortico-striatal synaptic defects and OCD-like behaviours in Sapap3-mutant mice. Nature. 2007; 448:894–900. [PubMed: 17713528]
17. Gee S, Ellwood I, Patel T, Luongo F, Deisseroth K, Sohal VS. Synaptic activity unmasks dopamine D2 receptor modulation of a specific class of layer V pyramidal neurons in prefrontal cortex. J Neurosci. 2012; 32:4959–4971. [PubMed: 22492051]
18. Zhao S, Ting JT, Atallah HE, Qiu L, Tan J, Gloss B, et al. Cell type-specific channelrhodopsin-2 transgenic mice for optogenetic dissection of neural circuitry function. Nat Methods. 2011; 8:745–752. [PubMed: 21985008]
19. Mukamel EA, Nimmerjahn A, Schnitzer MJ. Automated analysis of cellular signals from large-scale calcium imaging data. Neuron. 2009; 63:747–760. [PubMed: 19778505]
20. O'Connor DH, Peron SP, Huber D, Svoboda K. Neural activity in barrel cortex underlying vibrissa-based object localization in mice. Neuron. 2010; 67:1048–1061. [PubMed: 20869600]
21. Sanchez-Vives MV, McCormick DA. Cellular and network mechanisms of rhythmic recurrent activity in neocortex. Nat Neurosci. 2000; 3:1027–1034. [PubMed: 11017176]
22. Moore SJ, Turnpenny P, Quinn A, Glover S, Lloyd DJ, Montgomery T, et al. A clinical study of 57 children with fetal anticonvulsant syndromes. J Med Genet. 2000; 37:489–497. [PubMed: 10882750]
23. Rasalam AD, Hailey H, Williams JH, Moore SJ, Turnpenny PD, Lloyd DJ, et al. Characteristics of fetal anticonvulsant syndrome associated autistic disorder. Dev Med Child Neurol. 2005; 47:551–555. [PubMed: 16108456]
24. Christensen J, Gronborg TK, Sorensen MJ, Schendel D, Parner ET, Pedersen LH, et al. Prenatal valproate exposure and risk of autism spectrum disorders and childhood autism. JAMA. 2013; 309:1696–1703. [PubMed: 23613074]
25. Schneider T, Przewlocki R. Behavioral alterations in rats prenatally exposed to valproic acid: animal model of autism. Neuropsychopharmacology. 2005; 30:80–89. [PubMed: 15238991]
26. Schneider T, Roman A, Basta-Kaim A, Kubera M, Budziszewska B, Schneider K, et al. Gender-specific behavioral and immunological alterations in an animal model of autism induced by prenatal exposure to valproic acid. Psychoneuroendocrinology. 2008; 33:728–740. [PubMed: 18396377]
27. Bakker CE, Verheij C, Willemsen R, van der Helm R, Oerlemans F, Vermey M, et al. Fmr1 knockout mice: a model to study fragile X mental retardation. The Dutch-Belgian Fragile X Consortium. Cell. 1994; 78:23–33. [PubMed: 8033209]
28. Pletnikov MV, Ayhan Y, Nikolskaia O, Xu Y, Ovanesov MV, Huang H, et al. Inducible expression of mutant human DISC1 in mice is associated with brain and behavioral abnormalities reminiscent of schizophrenia. Mol Psychiatry. 2008; 13:173–186. 115. [PubMed: 17848917]
29. Hikida T, Jaaro-Peled H, Seshadri S, Oishi K, Hookway C, Kong S, et al. Dominant-negative DISC1 transgenic mice display schizophrenia-associated phenotypes detected by measures translatable to humans. Proc Natl Acad Sci U S A. 2007; 104:14501–14506. [PubMed: 17675407]
30. Clapcote SJ, Lipina TV, Millar JK, Mackie S, Christie S, Ogawa F, et al. Behavioral phenotypes of Disc1 missense mutations in mice. Neuron. 2007; 54:387–402. [PubMed: 17481393]
31. Kodama M, Fujioka T, Duman RS. Chronic olanzapine or fluoxetine administration increases cell proliferation in hippocampus and prefrontal cortex of adult rat. Biol Psychiatry. 2004; 56:570–580. [PubMed: 15476686]
32. Markram H, Rinaldi T, Markram K. The intense world syndrome--an alternative hypothesis for autism. Front Neurosci. 2007; 1:77–96. [PubMed: 18982120]
33. Gibson JR, Bartley AF, Hays SA, Huber KM. Imbalance of neocortical excitation and inhibition and altered UP states reflect network hyperexcitability in the mouse model of fragile X syndrome. J Neurophysiol. 2008; 100:2615–2626. [PubMed: 18784272]
34. Goncalves JT, Anstey JE, Golshani P, Portera-Cailliau C. Circuit level defects in the developing neocortex of Fragile X mice. Nat Neurosci. 2013; 16:903–909. [PubMed: 23727819]
35. Kawaguchi Y. Selective cholinergic modulation of cortical GABAergic cell subtypes. J Neurophysiol. 1997; 78:1743–1747. [PubMed: 9310461]

36. Xiang Z, Huguenard JR, Prince DA. Cholinergic switching within neocortical inhibitory networks. Science. 1998; 281:985–988. [PubMed: 9703513]

37. Pafundo DE, Miyamae T, Lewis DA, Gonzalez-Burgos G. Cholinergic modulation of neuronal excitability and recurrent excitation-inhibition in prefrontal cortex circuits: implications for gamma oscillations. J Physiol. 2013; 591:4725–4748. [PubMed: 23818693]

38. Dembrow NC, Chitwood RA, Johnston D. Projection-specific neuromodulation of medial prefrontal cortex neurons. J Neurosci. 2010; 30:16922–16937. [PubMed: 21159963]

39. Gil Z, Connors BW, Amitai Y. Differential regulation of neocortical synapses by neuromodulators and activity. Neuron. 1997; 19:679–686. [PubMed: 9331357]

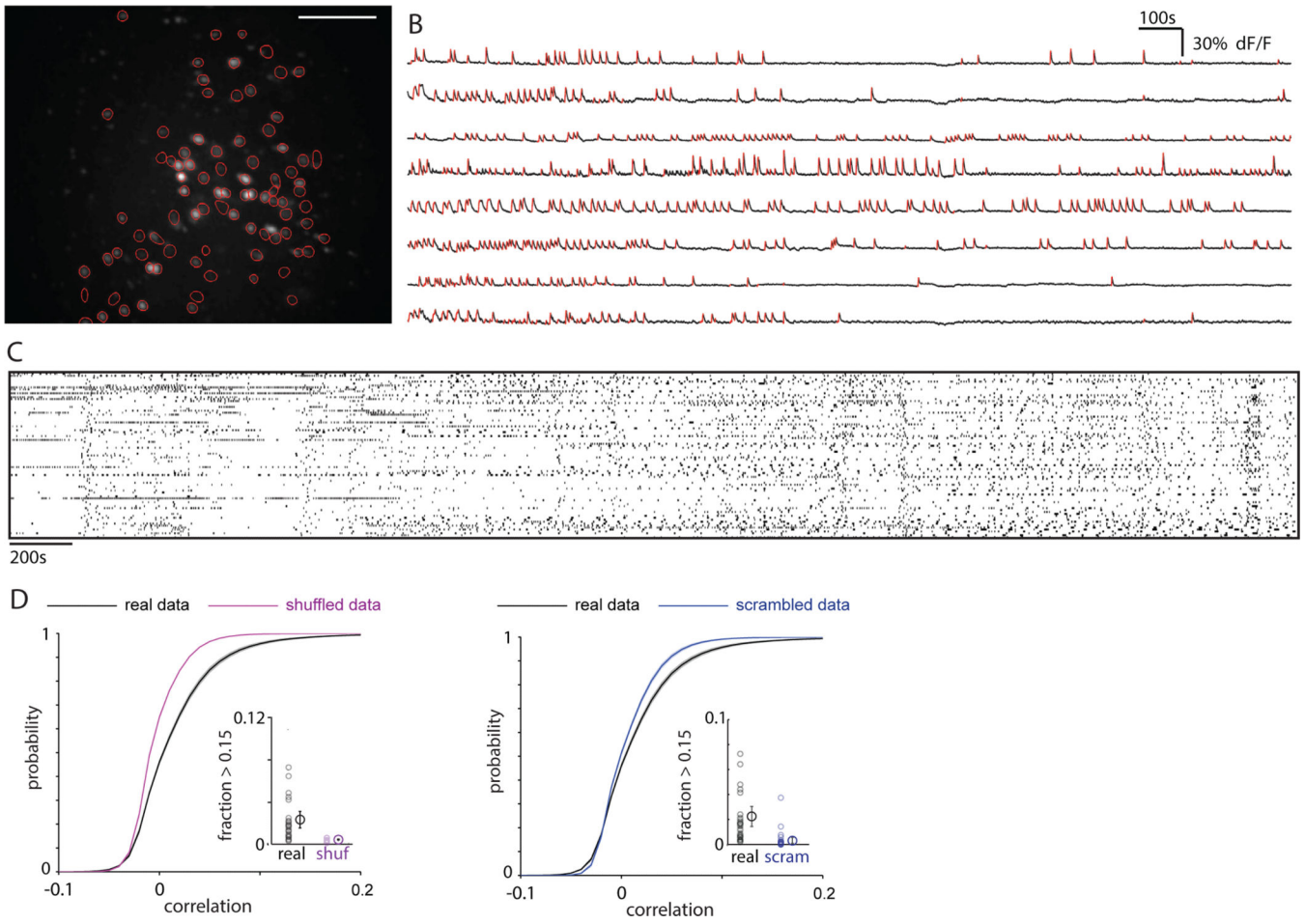

Figure 1. Single photon GCaMP imaging resolves simultaneous activity from many neurons in prefrontal slices

a, Regions of Interest (ROIs) obtained by an automated algorithm, showing the locations of neurons, superimposed on the maximum standard deviation projection of a GCaMP6s movie .

b, Sample GCaMP6s signals from 8 neurons (out of 84 total neurons imaged). Overlaid red lines indicate times when we detected that a neuron was active.

c, Example raster of spontaneous network activity for a single 60 min experiment with 84 neurons.

d, Cumulative probability distributions for correlations in real datasets (black line; n = 29 experiments from wild-type mice) vs. those observed in data shuffled by shifting each neuron's event train by a different random amount (“shuffled”, purple line) or by randomly reassigning the neuronal identity associated with each event (“scrambled”, blue line). Inset: the fraction of correlations > 0.15 are shown for real and shuffled / scrambled datasets. In each case, both the individual datapoints as well as the means and standard errors are shown.

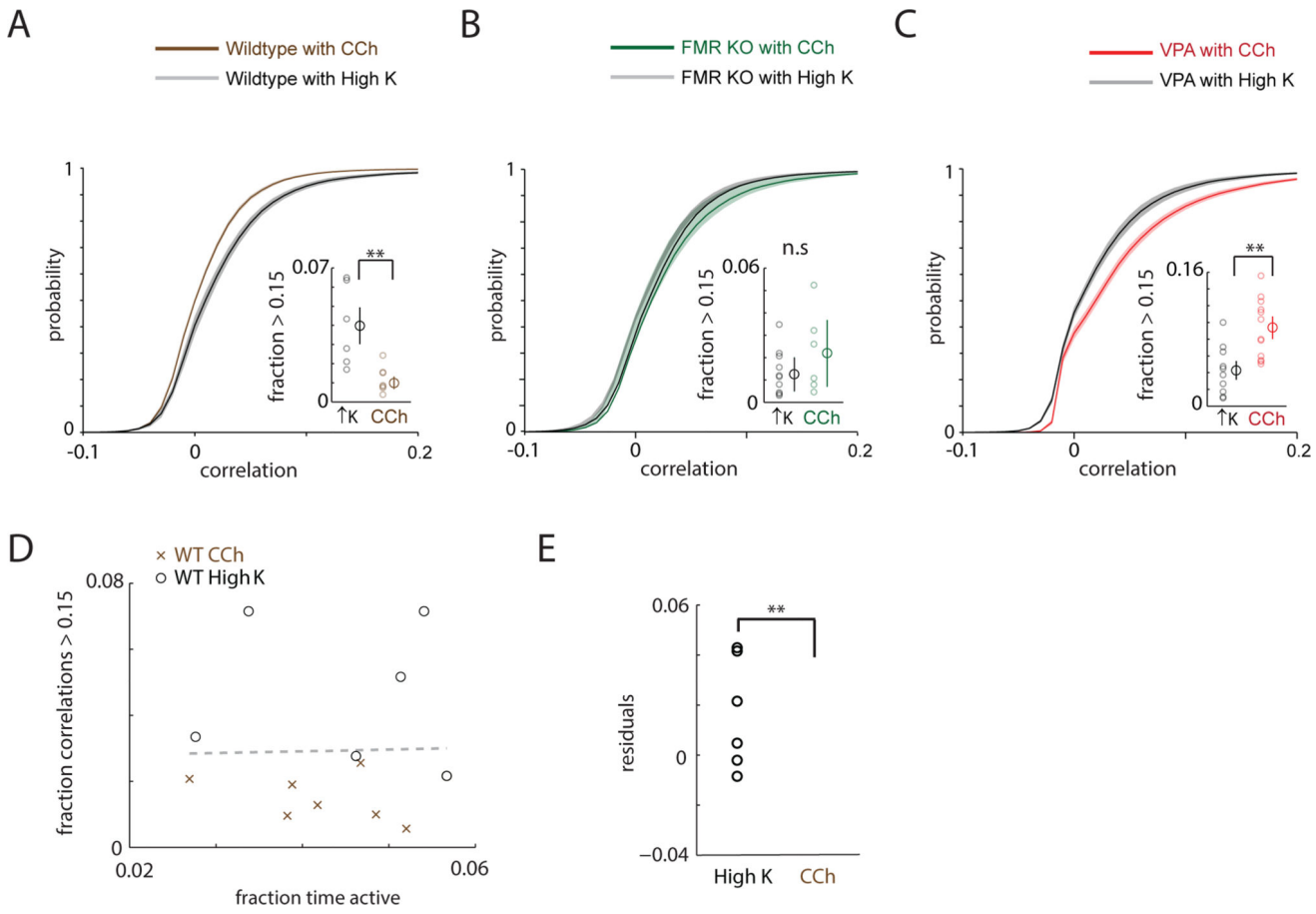

Figure 2. Cholinergic modulation decorrelates microcircuit activity in wild-type mice, but not in models of autism

a. Cumulative distribution of pairwise correlations for *FMR1* WT datasets using either 2 μM carbachol (n = 7) or high K^+ ACSF to elicit activity (n = 6). Inset: In carbachol, there are fewer strong correlations (>0.15) compared to high K^+ ACSF ($p < 0.01$).

b, Cumulative distribution plot for correlations recorded from *FMR1* KO mice in carbachol (green line) or high K^+ ACSF (black line). Inset: In carbachol, there is no reduction in strong correlations (>0.15), compared to high K^+ ACSF. Both individual datapoints as well as the means and standard errors are shown.

c, Cumulative distribution plot for correlations recorded from VPA-exposed mice in carbachol (red line) or high K^+ ACSF (black line). Inset: In carbachol, there are more strong correlations (>0.15), compared to high K^+ ACSF. Both individual datapoints as well as the means and standard errors are shown.

d, Scatterplot of the fraction of strong correlations as a function of the fraction of time active for WT datasets in carbachol (black O symbols) or high K^+ ACSF (brown X symbols). The gray dashed line represents a linear fit of all points (carbachol and high K^+ ACSF).

e, Residual values for the fractions of strong correlations, i.e. the difference between the actual values, and the fraction expected based on a linear relationship between activity and strong correlations, for carbachol (black) and high K^+ ACSF (brown) datasets. Even after accounting for a possible relationship between activity and strong correlations, the fraction

of strong correlations in high K^+ ACSF is still significantly greater than in carbachol. ** $p < 0.01$ by Wilcoxon rank sum test

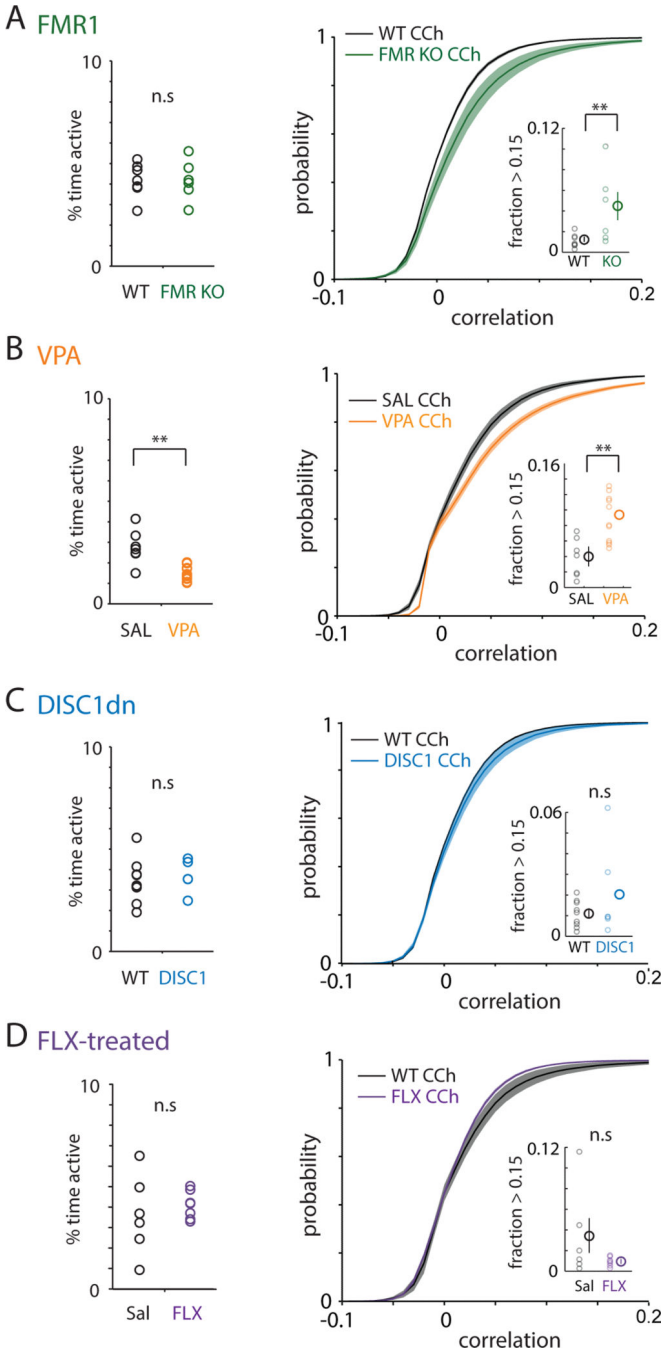

Figure 3. Autism models, but not DISC1 mutant or fluoxetine-treated mice, exhibit abnormally elevated correlations in carbachol

a, Left: Plot of the average amount of time each neuron was active for *FMR1* WT (filled black circles, left; n=7) or *FMR1* KO slices (filled green circles, right; n=6). ***Right***: Cumulative distribution of correlations, averaged over all experiments in *FMR1* WT (black; n=7) or *FMR1* KO slices (green; n=6). Inset shows fraction of strong correlations, i.e. values > 0.15 for each condition, and both individual datapoints as well as the means and standard errors are plotted.

b, Similar to *a*, but compares experiments in saline-exposed (black; n=9) or VPA-exposed slices (orange; n=12).

c, Similar to *a*, but compares experiments in control (black circles, left; n=8) vs. dominant negative DISC1 mutant mice (blue circles, right; n=6).

d, Similar to *a*, but compares experiments in saline-treated (black circles, left; n=6) compared to FLX-treated mice (purple circles, right; n=7).

** $p < 0.01$ by Wilcoxon ranksum test.

Table 1

List of all experiments along with summary statistics describing network activity.

	Genotype/Condition	Background	Bath condition	No. Slices	No. Mice	No. Cells	% time active	Fraction pairs > 0.15
	GCaMP6s							
VPA	VPA exposed	C57B16	2μM Carbacho 1	11	7	64 ± 2.3	1.4 ± 0.1	0.094 ± 0.010
	VPA exposed	C57B16	‘active’ ACSF	10	6	83 ± 2.3	3.1 ± 0.3	0.043 ± 0.009
	saline exposed controls	C57B16	2μM Carbacho 1	7	4	76 ± 4.2	2.8 ± 0.3	0.039 ± 0.009
FMR1	FMR1 KO	FVB1	2μM Carbacho 1	6	4	83 ± 1.8	4.3 ± 0.4	0.045 ± 0.015
	FMR1 WT	FVB1	2μM Carbacho 1	7	4	86 ± 1.8	4.2 ± 0.3	0.012 ± 0.003
	FMR1 KO	FVB1	‘active’ ACSF	12	7	85 ± 1.6	5.6 ± 0.4	0.026 ± 0.005
	FMR1 WT	FVB1	‘active’ ACSF	6	3	80 ± 2.4	4.5 ± 0.5	0.040 ± 0.009
FLX	Fluoxetine injected	C57B16	2μM Carbacho 1	8	6	85 ± 1.3	4.1 ± 0.2	0.010 ± 0.002
	Saline injected	C57B16	2μM Carbacho 1	6	5	78 ± 1.7	3.6 ± 0.8	0.033 ± 0.018
DISC1dn	CamKII::ttA / tetO - DISC1dn	C57B16	2μM Carbacho 1	6	3	86 ± 2.4	3.8 ± 0.3	0.020 ± 0.009
	tetO - DISC1dn/ +	C57B16	2μM Carbacho 1	2	2	86 ± 0.5	3.2 ± 0.1	0.016 ± 0.005
	CamKII :: ttA / +	C57Bl6	2μM Carbacho 1	4	3	83 ± 3.5	3.7 ± 0.8	0.011 ± 0.004
	+/+	C57Bl6	2μM Carbacho 1	3	3	89 ± 4.0	3.3 ± 0.5	0.008 ± 0.003

All values shown as mean with SEM

Each row describes a single experimental condition. Mice that correspond to controls and experimental manipulations (e.g. *FMR1* WT and KO mice) are listed together. In addition to the experimental condition, we present the background for all mice, the bath condition used to elicit activity (either carbachol or active ACSF), the number of cells in each experiment, the % time that each cell was active, and the fraction of pairwise correlations between neurons that exceed 0.15. All data show represent means across an experimental condition ± one S.E.M.